光学学报

基于分子间电荷转移效应的P3HT∶Y6基可近红外响应有机光电倍增探测器

胡依凡[1]，滑羽璐[2]，冀婷[1*]，石林林[2]，崔艳霞[2]，李国辉[2**]

[1]太原理工大学物理学院，山西 太原 030024；

[2]太原理工大学电子信息与光学工程学院，山西 太原 030024

摘要 通过在成本较低的活性层P3HT中引入少量在近红外波段有吸光能力的有机受体Y6制成倍增器件，Y6与P3HT发生分子间电荷转移，使得器件的响应波段拓展至1310 nm，在目前所报道的近红外倍增型有机光电探测器中具有明显优势。在空穴传输层与活性层之间引入原子级厚度的Al_2O_3，极大降低了器件的暗电流，将器件由只能反向偏压响应改善到能够正反双向偏压响应。Al_2O_3修饰后器件在860 nm处的外量子效率为800%，比探测率为5.6×10^{11} Jones；1310 nm处器件的外量子效率为80.4%，比探测率为5.13×10^{10} Jones。

关键词 探测器；分子间电荷转移；近红外波段；有机光电倍增探测器；双向偏压；界面修饰

中图分类号 O436 **文献标志码** A **DOI**：10.3788/AOS231612

1 引 言

光电探测器是一种能将入射光信号转化为电信号的光电子器件[1]，在火焰和辐射检测、图像传感[2]、健康监测[3]、光纤通信[4]等领域都有着广泛的应用。传统的光电探测器一般基于硅、锗、砷化镓等无机半导体材料进行制备，它们不仅制备过程复杂、成本高昂，而且机械柔韧性较差[5]。相比而言，有机光电探测器具有成本低、质量轻、易于大面积加工[6]等优势，且与柔性衬底有更好的兼容性[7]，在柔性电子皮肤、可穿戴设备、生物医学成像等新兴领域的应用前景广阔[8]。

目前，有机光电探测器发展迅速，已经可以探测紫外、可见、近红外波段的光信号[9-12]。许多领域如医学检测、食品监测对近红外探测的需求日益迫切，因此，可近红外响应的有机光电探测器成为研究的一大热点[13-14]。近年来，得益于窄带隙给体材料和非富勒烯受体材料的发展，近红外有机光电探测器得到了快速的发展[15-16]。基于陷阱辅助载流子隧穿机理的倍增型有机光电探测器由于外量子效率(EQE)大、响应度高受到了研究人员的重视[17-19]，可近红外响应的有机光电倍增探测器已有很多报道[20]。2021年，Han等[17]制备了以PBDB-9T∶Y6为活性层的器件，可以在300～900 nm波长范围内响应，在790 nm处外量子效率达到66，比探测率达到4.9×10^{12} Jones。2021年，Liu等[2]采用P3HT、BEH、PTB7-Th、F_6TCNNQ来制备倍增型有机光电探测器，器件可以在300～900 nm波长范围内响应，在850 nm处外量子效率达到150，响应度为0.1 A/W，比探测率达到8.8×10^{11} Jones。目前，近红外有机光电倍增探测器的研究取得了不错的进展，但活性层大多采用价格高昂的窄带隙给体及受体材料，这就提高了器件的成本。此外，已报道的近红外有机光电倍增探测器的探测波长大多在1000 nm以下[21-23]。

基于分子间电荷转移的近红外有机光电探测器，利用给体/受体材料分子间电荷转移(CT)吸收原理直接将吸收波段拓展至短波红外区域，但面临着吸收低、响应弱的问题，而采用倍增器件结构可以放大微弱的光电流信号，提升器件的性能[24]。据此，本文制备了结构为ITO/PEDOT∶PSS/Al_2O_3/P3HT∶Y6(100∶1)/Al的倍增型近红外有机光电探测器，通过在成本较低的活性层P3HT中少量引入在近红外波段有吸光能力的有机受体Y6，实现了器件在近红外波段的响应，降低了器件的成本，并通过P3HT与Y6之间的分子间电荷转移效应，器件的响应波段可拓展至1310 nm。同时，在器件中加入原子级厚度的Al_2O_3，有效抑制了暗

收稿日期：2023-09-28；**修回日期**：2023-11-14；**录用日期**：2023-11-30；**网络首发日期**：2023-12-12

基金项目：国家自然科学基金(U21A20496，61922060，62174117，62205235，12104334)、山西省重点研发计划项目(202102150101007)、山西省自然科学基金(20210302123154，20210302123169)、山西浙大新材料与化工研究院研发项目(2021SX-FR008，2022SX-TD020)、中央引导地方科技发展资金项目(YDZJSX2021A012)、山西省省筹资金资助回国留学人员科研项目(2021-033)、吕梁市人才引进专项(Rc2020206，Rc2020207)

通信作者：*jiting@tyut.edu.cn；**liguohui@tyut.edu.cn

电流，从而将器件由只能反向偏压响应改善到能够正反双向偏压响应。研究结果表明：当光功率密度为 3.8×10^{-4} mW/cm^{2}时，器件在 860 nm 处的外量子效率为 800%，比探测率为 5.6×10^{11} Jones；当光功率密度为 3.67×10^{-2} mW/cm^{2}时，器件在 1310 nm 处的外量子效率为 80.4%，比探测率为 5.13×10^{10} Jones。这些性能在目前所报道的近红外倍增型有机光电探测器中具有一定优势。

2 实　　验

2.1 样品制备

氧化铟锡（ITO）基底的处理：采用商业化刻蚀后带有 ITO 图形的玻璃衬底，制备出有效面积为 0.2 cm×0.2 cm 的光电倍增探测器。将 ITO 用洗洁精和洗涤剂搓洗以去除表面污渍，随后用去离子水冲洗，并分别置于丙酮、无水乙醇、异丙醇溶液中超声 15 min，用氮气吹干后移到手套箱。

空穴传输层 PEDOT∶PSS（聚(3,4-乙烯二氧噻吩)-聚苯乙烯磺酸）的制备：首先，将 PEDOT∶PSS 与无水乙醇按照 1∶9 的体积比稀释，用 1 mL 针管吸取一定量 PEDOT∶PSS 并加装合适的滤头，旋涂在处理好的 ITO 基底上，转速为 9000 r/min，匀胶时间为 30 s；然后，置于 120 ℃热台上退火 15 min。

Al_2O_3界面修饰层的制备：利用原子层沉积设备在真空 150 ℃下使 $Al(CH_3)_3$ 和 H_2O 交替反应，以 0.1 nm/cycle 的速率沉积厚度为 0.8 nm 的 Al_2O_3，结束后冷却 3 min 待用。

活性层的制备：将 P3HT（3-己基取代聚噻吩）和 Y6(2,20-((2Z,20Z)-((12,13-双(2-乙基己基)-3,9-双十一烷-12,13-二氢-[1,2,5]噻二唑[3,4-e]噻吩并[2″,30′∶4′,50]噻吩并[20,30∶4,5]吡咯并[3,2-g]噻吩并[20,30∶4,5]噻吩并[3,2-b]吲哚-2,10-二基)双-(2-甲烯基))-(3-1,1-甲烯丙二腈)-5,6-二氟茚酮))按照 100∶1 的质量比溶于邻二氯苯，配置 40 mg/mL 的溶液。将 30 μL 的 P3HT∶Y6 溶液旋涂在 ITO/PEDOT∶PSS/Al_2O_3 的玻璃片上，转速为 1000 r/min，时间为 30 s，旋涂完毕后立即置于 80 ℃热台退火 20 s，结束后冷却 3 min 待用。

金属电极的制备：利用蒸镀设备在 10^{-4} Pa 的高真空下蒸镀 100 nm 厚度的 Al 电极。

2.2 测试与表征

对制备的近红外有机光电倍增探测器的性能表征指标主要有：光照及暗态下的电流密度-电压（*J*-*V*）曲线、外量子效率、响应度、噪声电流、比探测率、线性动态范围、瞬态响应曲线、紫外-可见-近红外吸收光谱及膜厚等。

光电测试系统所在实验环境为密闭且室温状态，利用数字源表 Keithley 2400 获得器件的电流，光源采用不同波长的 LED 光源（如 375、505、660、850 nm）及激光器（如 980 nm、1310 nm）；外量子效率和响应度的测试是将器件放置在暗箱屏蔽箱中，ITO 作为器件阳极接电源正极，Al 作为阴极接电源负极，对数字源表 Keithley 2400 施加不同电压，并利用飞秒激光器作为光源，使用衰减片将光强衰减到指定大小，采集暗电流和不同光源下的亮态 *J*-*V* 曲线，并通过计算获得外量子效率和响应度数据（数据已作背景扣除）。利用频谱分析仪与安捷伦 B2961 连接测试噪声电流，由安捷伦 B2900A 采集数据；利用信号发生器和安捷伦 B2900A 测试瞬态响应曲线；利用分光光度计采集紫外-可见-近红外吸收光谱，同时结合自动宏观角分辨光谱仪 R1 辅助测试器件的透射谱及反射谱；利用台阶仪测试薄膜厚度。

3 分析与讨论

3.1 Al_2O_3界面修饰层在器件中的作用

制备了 ITO/PEDOT∶PSS/Al_2O_3/P3HT∶Y6(100∶1)/Al（Al_2O_3 修饰器件）以及 ITO/PEDOT∶PSS/P3HT∶Y6(100∶1)/Al（标准器件）两种器件，器件结构如图 1(a)所示。将两种器件分别在暗态及 850 nm 光源（1.27 mW/cm^2）下进行测试表征，结果如图 1(b)所示。Al_2O_3修饰界面后，器件在正向及反向偏压下的暗电流密度均有大幅降低，如：在正向 15 V 偏压下，暗电流密度从 2.0×10^3 mA/cm^{2}降低到 8.6×10^{-3} mA/cm^2，降低了 5 个数量级；在反向 −15 V 偏压下，暗电流密度从 1.7×10^{-1} mA/cm^{2}降低到 9.7×10^{-3} mA/cm^2，降低了 1 个数量级。通过测试结果发现，加 Al_2O_3界面修饰层后，器件的光电流密度也有所降低，但其降低幅度远小于暗电流密度的降低幅度。标准器件及 Al_2O_3修饰器件的亮暗电流比（J_L/J_D）如图 1(c)所示。正向偏压下标准器件没有响应，而 Al_2O_3修饰器件在正反偏压下都有响应，改善了标准器件正向不响应的缺点，并且在 15 V 正向偏压下实现了 3×10^3 的亮暗电流比（J_L/J_D），优于反向偏压的亮暗电流比，具有更好的性能。

为了分析工作机理及 Al_2O_3界面修饰层的作用，对能带图进行分析，如图 1(d)所示。结合本课题组之前的工作[25]可知，P3HT 的最高占据分子轨道（HOMO）能级为 −5.1 eV，非常接近 PEDOT∶PSS 的费米能级（−5.0 eV），并在阳极一侧产生欧姆接触，因此正向偏压下空穴可以从 ITO 一侧无障碍注入，导致标准器件在正向偏压下暗电流较高。在 Al 阴极附近，由于 P3HT 和 Al 之间存在 0.8 eV 的功函数差，建立了向下弯曲的肖特基结，反向偏压下空穴由 Al 阴极注入时被势垒阻挡，因此标准器件的暗态 *J*-*V* 曲线表现出单边导电特性。光照下，当对标准器件施加反向偏压时，大量的光生电子被电子陷阱俘获，并在外加电压的作用下向阴极漂移，积累在 P3HT∶Y6/Al 阴极界面，从而引起肖特基势垒宽度窄

化，利于外电路空穴大量隧穿注入，进而产生光电流，这个过程即为电子陷阱辅助空穴隧穿。在正向偏压下，注入电流较大，响应信号不明显，所以正向偏压下标准器件无响应。

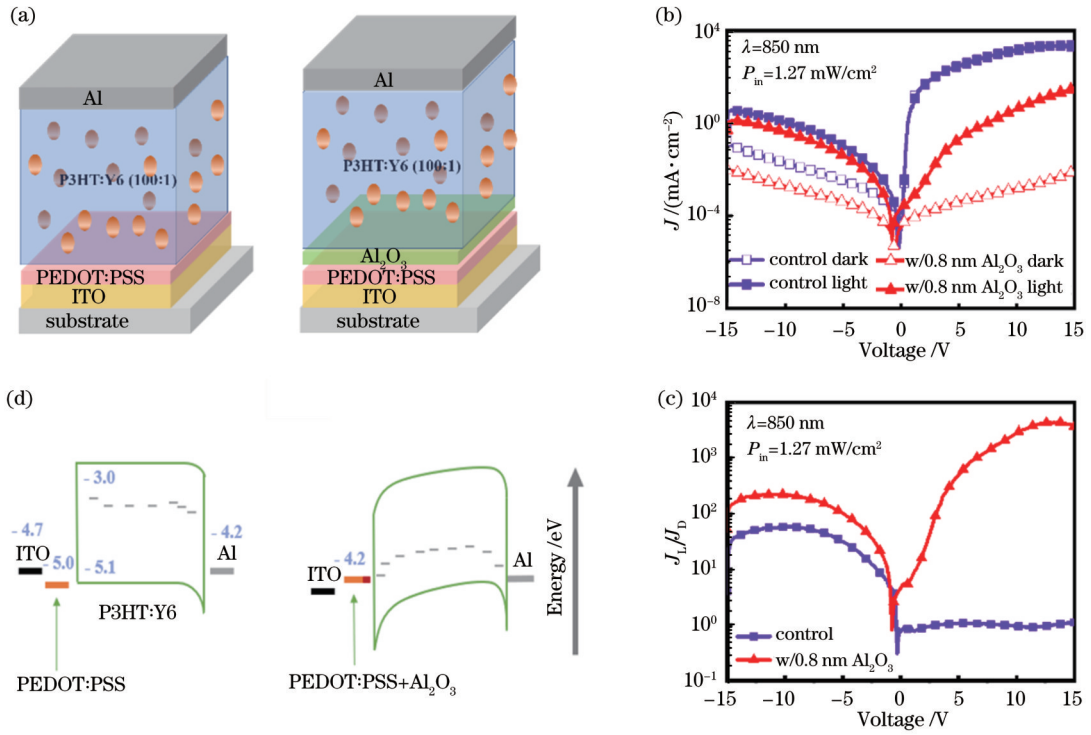

图 1　不含与含 Al_2O_3 界面修饰层的器件结构及性能。(a)两种类型器件的结构；(b)两种类型器件在 850 nm(1.27 mW/cm²)下的 J-V 曲线；(c)两种类型器件在 850 nm(1.27 mW/cm²)下的亮暗电流比曲线；(d)两种类型器件的能级图

Fig. 1　Structure and performance of devices without and with Al_2O_3. (a) Structure diagram of two devices; (b) J-V curves of two devices at 850 nm (1.27 mW/cm²); (c) light-to-dark current ratio curves of two devices at 850 nm (1.27 mW/cm²); (d) energy level diagrams of two devices

使用 0.8 nm 厚的 Al_2O_3 修饰后，PEDOT∶PSS 的功函数值出现明显变化，由 5.0 eV 减小到 4.2 eV[25]。P3HT 和 Al_2O_3 修饰后的 PEDOT∶PSS 的功函数相差 0.8 eV，形成了如图 1(d)所示的阳极肖特基结，在正向偏压下可阻挡空穴注入，有效抑制暗电流，改善标准器件正向不响应的缺点。由于活性层 P3HT∶Y6 与 Al 电极界面处形成向下弯曲的肖特基结，可有效阻止空穴的注入，在反向偏压下也有明显的亮暗电流差。测试结果表明，在反向偏压下，加 Al_2O_3 界面修饰层器件的暗电流相较于标准器件有所降低，这是因为引入的 Al_2O_3 使得阳极附近存在金属-绝缘体-半导体(MIS)隧穿结，可以进一步阻止其他载流子注入外电路。光照条件下，对 Al_2O_3 修饰器件施加正向偏压时，Al_2O_3 与 P3HT∶Y6 界面处形成向下弯曲的 MIS 隧穿结，在外加电压下，光生电子被电子陷阱俘获，漂移运动至阳极附近，引起肖特基势垒窄化，外电路的空穴在外加电压下由阳极 ITO 一侧向阴极 Al 隧穿注入，从而产生可区分的光电流信号。当施加反向偏压时，其机理与不加界面层的机理基本一致，这是因为 Al_2O_3 界面修饰层厚度为原子级厚度 0.8 nm，MIS 隧穿结不会影响载流子的传输和收集。

3.2　器件性能表征

接下来对 Al_2O_3 修饰器件进行性能表征。图 2(a)所示为飞秒激光(功率密度为 1 μW/cm²)测量器件在不同波长光照射下的外量子效率谱，图 2(b)、(c)所示为器件在 375、505、660、850、980、1120、1208、1310 nm 光照射下的瞬态响应曲线。可以看到，器件在 300～1310 nm 范围内具有宽谱响应。图 2(a)表明，器件在 500 nm 处的外量子效率达到 2.62×10^3，且响应光谱在 320～940 nm 范围的外量子效率都在 100% 以上。器件在 15 V 偏压下 500 nm 处外量子效率达到 10^3，主要是因为入射光在阳极附近很快被高效吸收，产生更多的光生载流子，从而促进阳极附近的光电倍增行为。此外，进一步表征了器件的 −3 dB 截止频率，如图 2(d)所示。器件的截止频率为 3.5 Hz，该截止频率下计算的响应时间与 850 nm 处由瞬态响应计算的响应时间一致。

此外，还测试了器件在 505、860、1310 nm 光照射下器件的动态范围、外量子效率、响应度和比探测率曲线，如图 3 所示，其中动态范围(R_{DR})的计算公式如式(1)所示。

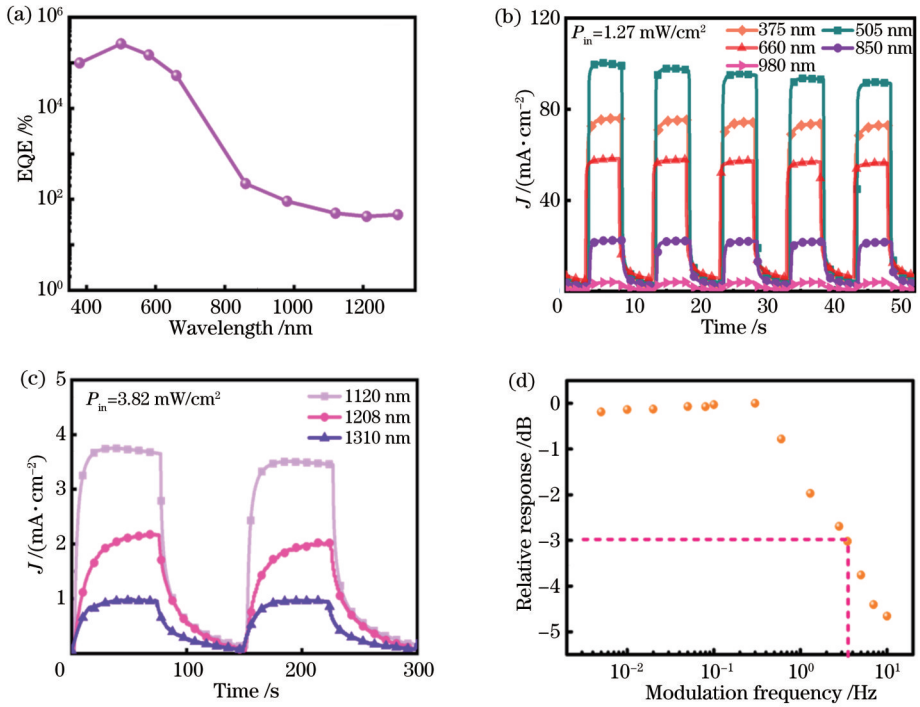

图 2 Al_2O_3修饰器件在 15 V 偏压下的相关表征。(a)外量子效率光谱;(b)瞬态响应曲线;(c)1120、1208、1310 nm 光源照射下的瞬态响应曲线;(d)调制光源下的$f_{-3\,dB}$测试结果

Fig. 2 Characterization of Al_2O_3 modified device under 15 V bias voltage. (a) EQE spectrum; (b) transient response curves; (c) transient response curves under 1120, 1208, and 1310 nm light source irradiation; (d) $f_{-3\,dB}$ measurement results under modulated light source

$$R_{DR}=20\log\left(\frac{P_{upper}}{P_{lower}}\right), \tag{1}$$

式中:P_{upper}和P_{lower}分别表示动态范围内可探测光强的上限和下限。器件在 505 nm 处的弱光探测极限可达 7.8 nW/cm²,通过测试发现器件在 505 nm、15 V 偏压下具有 125 dB 的动态范围,当光功率密度为 7.8×10^{-6} mW/cm²时,外量子效率达到 1.3×10^{5}%,响应度(R)达到 5.2×10^{2} A/W,比探测率(D^*)为 5.4×10^{13} Jones。器件在 860 nm 近红外波长处的动态范围为 90 dB,当光功率密度为 3.8×10^{-4} mW/cm²时,外量子效率可达 800%,比探测率为 5.6×10^{11} Jones。器件在 1310 nm 处,当光功率密度为 3.67×10^{-2} mW/cm²时,外量子效率达到 80.4%,响应度达到 0.85 A/W,比探测率可达 5.13×10^{10} Jones。此外,505 nm 和 860 nm 两个波段的外量子效率和响应度随入射光功率密度的变化趋势有一定差异,这主要是因为器件的活性层在 505 nm 处的吸收最强[图 4(b)],随着光功率密度的增大,其光电流密度会大于 860 nm 下的光电流密度,所以 505 nm 处的外量子效率和响应度变化幅度会大于 860 nm 处。综上,所制备的器件在响应波长方面具有明显优势,其他性能也与目前报道的近红外有机光电倍增探测器的水平相当。

3.3 器件机理分析

为了分析器件在长波段响应的原因,制备了Al_2O_3修饰的 P3HT∶Y6 活性层器件,并和纯 P3HT 作为活性层的器件进行对比分析,结果如图 4(a)所示。纯 P3HT 器件在 660 nm 光源下的瞬态响应明显低于 P3HT∶Y6 器件,表明掺杂的 Y6 可以作为电子陷阱有效促进空穴从外电流大量注入。在 850 nm 光照下,纯 P3HT 作为活性层的器件已经没有响应,主要原因是 P3HT 材料本身在 800 nm 已经不吸光,故无法响应到 850 nm。因此,少量 Y6 的加入可使器件在长波段产生响应。

为了更好地分析器件性能产生的机理,测试了拉曼光谱和光致发光光谱。图 4(c)所示为 P3HT 薄膜及 P3HT∶Y6 共混薄膜(质量比为 100∶1)的拉曼光谱。测试结果表明,P3HT 的拉曼特征峰位于 1377 cm^{-1}和 1445 cm^{-1},而混合薄膜 P3HT∶Y6 的拉曼特征峰位于 1377 cm^{-1}和 1446 cm^{-1},这是因为 C═C 拉伸引起峰位移动,共混膜 P3HT∶Y6 相较于纯 P3HT 膜的拉曼位移移动了 1 cm^{-1},故推测 P3HT 和 Y6 之间发生了相互作用[26-27]。除此之外,还测试了 325 nm 激光照射下的光致发光光谱,结果如图 4(d)所示。结果表明,P3HT 与 P3HT∶Y6 两种体系中存在不同的激发机理,P3HT 的发光峰位于 709 nm,而 P3HT∶Y6 共混膜的发光峰位于 707 nm,发生了蓝移且强度变弱,说明 Y6 作为受体引入会导致荧光猝灭现象,表明分子间存在相互作用[28],发生了电荷转移,复合物的形成导致它们的光学

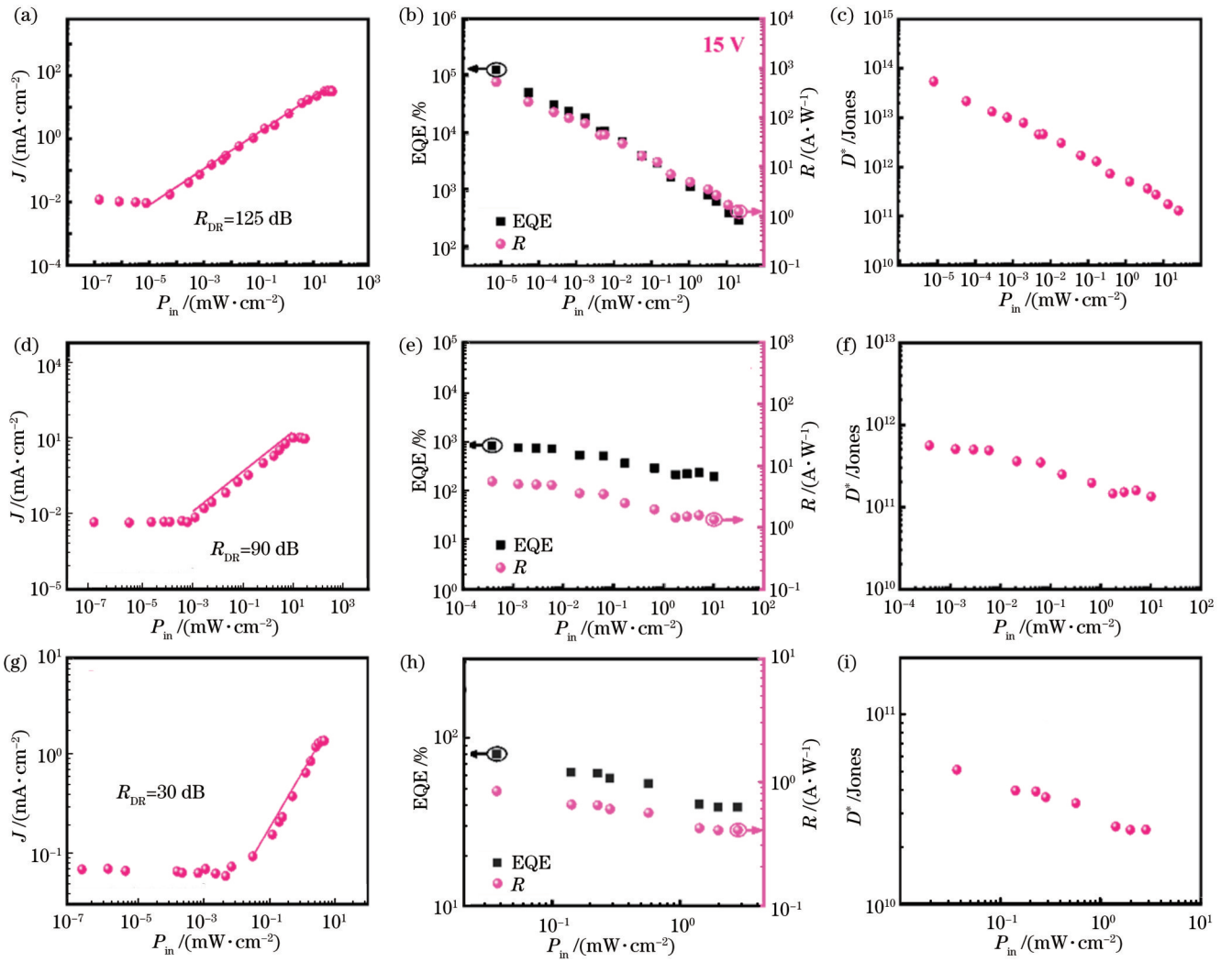

图 3 Al_2O_3修饰器件在不同光强下的相关表征。(a)505 nm 光源下的动态范围;(b)505 nm 光源下动态范围内的外量子效率和响应度;(c)505 nm 光源下动态范围内的比探测率;(d)860 nm 光源下的动态范围;(e)860 nm 光源下动态范围内的外量子效率和响应度;(f)860 nm 光源下动态范围内的比探测率;(g)1310 nm 光源下的动态范围;(h)1310 nm 光源下动态范围内的外量子效率和响应度;(i)1310 nm 光源下动态范围内的比探测率

Fig. 3 Characterizations of Al_2O_3 modified device under different light intensities. (a) Dynamic range under 505 nm light source; (b) EQE and responsibility under 505 nm light source within dynamic range; (c) specific detectivity under 505 nm light source within dynamic range; (d) dynamic range under 860 nm light source; (e) EQE and responsibility under 860 nm light source within dynamic range; (f) specific detectivity under 860 nm light source within dynamic range; (g) dynamic range under 1310 nm light source; (h) EQE and responsibility under 1310 nm light source within dynamic range; (i) specific detectivity under 1310 nm light source within dynamic range

性质发生了变化,而蓝移的出现是由激子态的变化引起的[29-31]。

图 4(b)所示为纯 P3HT 薄膜、纯 Y6 薄膜及混合薄膜 P3HT∶Y6 的吸收光谱。P3HT 在 520 nm 有最高的吸收峰,Y6 在 400~1000 nm 范围内有吸收且在 855 nm 波长处吸收最强,由于 Y6 能弥补 P3HT 在近红外不响应的缺点,因此当在 P3HT 中加入少量 Y6(质量比为 100∶1)时,除了在 520 nm 处有一个吸收峰外,在 785 nm 处也出现一个吸收峰,可以看出,加入 Y6 后,活性层在宽谱范围内都有吸收,且 P3HT∶Y6 共混薄膜在长波段的吸收高于 P3HT 和 Y6 单层薄膜,P3HT∶Y6 共混薄膜为活性层的器件可探测波长至 1310 nm 的光。分析推测,P3HT 与 Y6 之间发生了分子间电荷转移,形成了 CT 激子[29]。CT 是给体材料的 HOMO 和受体材料的最低未占据分子轨道(LUMO)相互作用的结果。如图 4(e)所示,光照下,电子从给体分子的 HOMO 转移到受体分子的 LUMO。由于 CT 激子所需能量较小,给体和受体的混合物可以吸收比各自带隙能量小的光子,从而实现对更长波段的光响应[32-33]。但是,CT 只存在于给体与受体接触的界面,其吸收能量比分子内吸收小两个量级,导致在长波段的吸收很弱,光电流信号很微弱。由于所设计器件

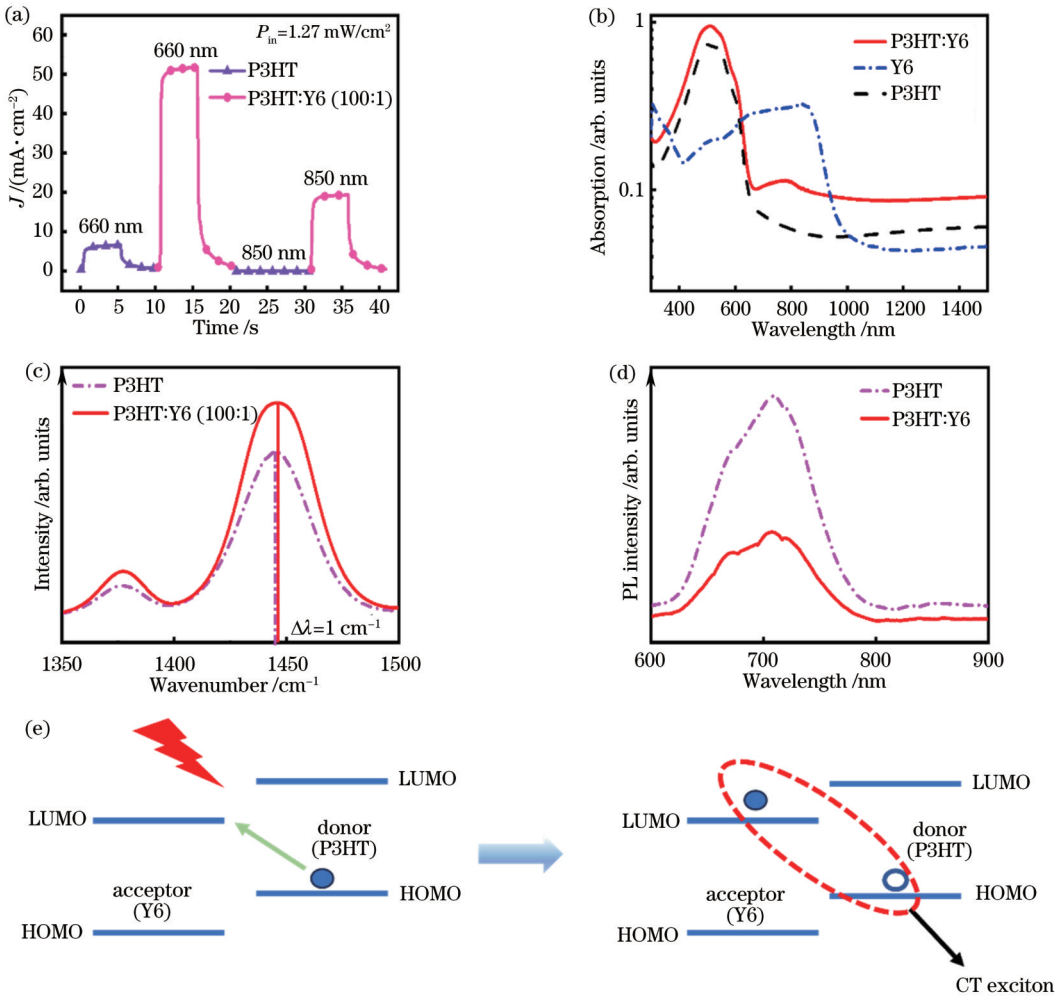

图 4　器件的机理分析图。(a)纯 P3HT 器件及 P3HT∶Y6 器件的瞬态响应曲线；(b)P3HT、Y6 及 P3HT∶Y6(100∶1)的吸收光谱；(c)P3HT 和 P3HT∶Y6(100∶1)的拉曼光谱；(d)P3HT 和 P3HT∶Y6(100∶1)在 325 nm 光源激发时的光致发光光谱；(e)分子间电荷转移形成原理示意图

Fig. 4　Mechanism analysis diagram of the device. (a) Transient response curves of pure P3HT thin film as active layer and Al_2O_3 modified devices; (b) absorption spectra of P3HT, Y6, and P3HT∶Y6 (100∶1); (c) Raman spectra of P3HT and P3HT∶Y6 (100∶1); (d) photoluminescence spectra of P3HT and P3HT∶Y6 (100∶1) excited by a 325 nm light source; (e) principle schematic of intermolecular charge transfer formation

采用倍增结构，可放大微弱的光电流信号，且在器件中引入了 Al_2O_3 界面修饰层，极大降低了暗电流，因此由 CT 吸收产生的长波段微弱光电流信号得以显现。

基于上述测试与分析，验证了器件的近红外性能主要来源于 Y6 的掺杂，并且通过采用 P3HT∶Y6 作为活性层，利用 Y6 的红外吸收特性以及 P3HT 与 Y6 之间的相互作用，实现了在近红外区域的高灵敏探测。

4　结　　论

制备了一种结构为 ITO/PEDOT∶PSS/Al_2O_3/P3HT∶Y6/Al 的低成本、高响应度的近红外有机光电倍增探测器，通过加入 Al_2O_3 作为界面修饰层，显著降低了器件的暗电流，得到能够正反偏压双向响应的器件。在活性层中添加少量的 Y6 可实现紫外-可见-近红外的宽光谱响应，基于 P3HT 和 Y6 之间发生的分子间电荷转移作用，响应波长可拓展至 1310 nm。器件在 860 nm 处的外量子效率可达 800%，比探测率为 5.6×10^{11} Jones；器件在 1310 nm 处的外量子效率达到 80.4%，比探测率可达 5.13×10^{10} Jones。这些性能在已报道的近红外有机光电倍增探测器中具有一定优势，可促进低成本近红外有机光电倍增探测器的发展。

参　考　文　献

[1] Guo D C, Yang L Q, Li J, et al. Panchromatic photomultiplication-type organic photodetectors with planar/bulk heterojunction structure[J]. Science China Materials, 2023, 66(3): 1172-1179.

[2] Liu M, Wang J, Zhao Z J, et al. Ultra-narrow-band NIR photomultiplication organic photodetectors based on charge injection narrowing[J]. The Journal of Physical Chemistry Letters, 2021, 12(11): 2937-2943.

[3] Nath D, Dey P, Joseph A M, et al. Zero bias high responsive visible organic photodetector based on pentacene and C_{60}[J].

Optics & Laser Technology, 2020, 131: 106393.

[4] Agostinelli T, Caironi M, Natali D, et al. A planar organic near infrared light detector based on bulk heterojunction of a heteroquaterphenoquinone and poly [2-methoxy-5- (2′-ethyl-hexyloxy) -1, 4-phenylene vinylene] [J]. Journal of Applied Physics, 2008, 104(11): 114508.

[5] Zhou X K, Yang D Z, Ma D G, et al. Ultrahigh gain polymer photodetectors with spectral response from UV to near-infrared using ZnO nanoparticles as anode interfacial layer[J]. Advanced Functional Materials, 2016, 26(36): 6619-6626.

[6] Yang L Q, Guo D C, Li J, et al. Low-cost copper electrode for high-performance panchromatic multiplication-type organic photodetectors with optical microcavity effect[J]. Advanced Functional Materials, 2022, 32(20): 2108839.

[7] Wang J B, Zheng Q D. Enhancing the performance of photomultiplication-type organic photodetectors using solution-processed ZnO as an interfacial layer[J]. Journal of Materials Chemistry C, 2019, 7(6): 1544-1550.

[8] 翁思远, 蒋大勇, 赵曼. P3HT∶PC61BM作为活性层制备无机/有机异质结光电探测器的研究[J]. 光学学报, 2022, 42(13): 1304001.
Weng S Y, Jiang D Y, Zhao M. P3HT∶PC61BM as active layer for preparation of inorganic/organic heterojunction photodetector[J]. Acta Optica Sinica, 2022, 42(13): 1304001.

[9] Zhang X R, Jiang J Z, Feng B G, et al. Organic photodetectors: materials, device, and challenges[J]. Journal of Materials Chemistry C, 2023, 11(37): 12453-12465.

[10] Zhao Z J, Xu C Y, Niu L B, et al. Recent progress on broadband organic photodetectors and their applications[J]. Laser & Photonics Reviews, 2020, 14(11): 2000262.

[11] Yang D Z, Ma D G. Development of organic semiconductor photodetectors: from mechanism to applications[J]. Advanced Optical Materials, 2019, 7(1): 1800522.

[12] Sun J, Peng K J, Zhu L, et al. Ultraviolet photodetector with bandpass characteristic based on a blend of PVK and PBD[J]. Chinese Optics Letters, 2011, 9(5): 052501.

[13] 薛晓梦, 马海菲, 郝群, 等. 高载流子迁移率胶体量子点红外探测器[J]. 光学学报, 2023, 43(22): 2204002.
Xue X M, Ma H F, Hao Q, et al. Infrared detectors of high carrier mobility colloidal quantum dots[J]. Acta Optica Sinica, 2023, 43(22): 2204002.

[14] 郝群, 唐鑫, 陈梦璐. 硫汞族量子点红外光电探测技术[J]. 光学学报, 2023, 43(15): 1500001.
Hao Q, Tang X, Chen M L. Infrared optoelectrical detection technology based on mercury chalcogenide colloidal quantum dots[J]. Acta Optica Sinica, 2023, 43(15): 1500001.

[15] Winkler L C, Kublitski J, Benduhn J, et al. Photomultiplication enabling high-performance narrowband near-infrared organic photodetectors[J]. Advanced Electronic Materials, 2023, 9(9): 2201350.

[16] Li Q Y, Guo Y L, Liu Y Q. Exploration of near-infrared organic photodetectors[J]. Chemistry of Materials, 2019, 31(17): 6359-6379.

[17] Han S G, Lee H, Choi W, et al. Photomultiplication-type organic photodetectors with fast response enabled by the controlled charge trapping dynamics of quantum dot interlayer[J]. Advanced Functional Materials, 2021, 31(31): 2102087.

[18] 安涛, 吴禧梅, 刘欣颖. 基于双掺杂C_{60}∶DDQ陷阱的倍增型有机光电探测器[J]. 光子学报, 2020, 49(10): 1025001.
An T, Wu X M, Liu X Y. Multiplying organic photodetector based on double-doped C_{60}∶DDQ trap[J]. Acta Photonica Sinica, 2020, 49(10): 1025001.

[19] An T, Liu X Y. Broadband organic color photodetectors with high gain based on C_{60}-doped tri-phase bulk heterojunction[J]. Journal of Materials Science: Materials in Electronics, 2020, 31(4): 2757-2765.

[20] 高秀云, 张叶, 崔艳霞, 等. 有机光电倍增探测器研究进展[J]. 激光与光电子学进展, 2018, 55(7): 070001.
Gao X Y, Zhang Y, Cui Y X, et al. Research progress in organic photomultiplication photodetector[J]. Laser & Optoelectronics Progress, 2018, 55(7): 070001.

[21] Tao S Z, Yang D Z, He G, et al. Photomultiplication-type perovskite photodetectors base on air-processed perovskite films [J]. Organic Electronics, 2023, 118: 106800.

[22] Yang K X, Zhao Z J, Liu M, et al. Employing liquid crystal material as regulator to enhance performance of photomultiplication type polymer photodetectors[J]. Chemical Engineering Journal, 2022, 427: 131802.

[23] Wang W B, Zhang F J, Bai H T, et al. Photomultiplication photodetectors with P3HT: fullerene-free material as the active layers exhibiting a broad response[J]. Nanoscale, 2016, 8(10): 5578-5586.

[24] Kublitski J, Fischer A, Xing S, et al. Enhancing sub-bandgap external quantum efficiency by photomultiplication for narrowband organic near-infrared photodetectors[J]. Nature Communications, 2021, 12: 4259.

[25] Shi L L, Zhu Y Z, Li G H, et al. Atomic-level chemical reaction promoting external quantum efficiency of organic photomultiplication photodetector exceeding 10^8% for weak-light detection[J]. Science Bulletin, 2023, 68(9): 928-937.

[26] Yamamoto J, Furukawa Y. Raman characterization and electrical properties of poly (3-hexylthiophene) doped electrochemically in an ionic liquid-gated transistor geometry[J]. Organic Electronics, 2016, 28: 82-87.

[27] Stylianakis M M, Stratakis E, Koudoumas E, et al. Organic bulk heterojunction photovoltaic devices based on polythiophene-graphene composites[J]. ACS Applied Materials & Interfaces, 2012, 4(9): 4864-4870.

[28] Wang T, Lu Y, Xu L, et al. π-conjugated poly (3-hexylthiophene-2, 5-diyl) thin film as a SERS substrate for molecule detection application[J]. Journal of Materials Science, 2022, 57(35): 16965-16973.

[29] Yin H, Tian T, Zhang R X, et al. High-performance broadband photodetectors based on asymmetric all-carbon nano-heterostructures[J]. ACS Applied Nano Materials, 2023, 6(13): 11934-11943.

[30] Xu Z H, He M, Wu Q K, et al. Ultrafast charge transfer 2D MoS_2/organic heterojunction for sensitive photodetector[J]. Advanced Science, 2023, 10(12): 2207743.

[31] Iqbal M A, Liaqat A, Hussain S, et al. Ultralow-transition-energy organic complex on graphene for high-performance shortwave infrared photodetection[J]. Advanced Materials, 2020, 32(37): 2002628.

[32] Kim J H, Liess A, Stolte M, et al. An efficient narrowband near-infrared at 1040 nm organic photodetector realized by intermolecular charge transfer mediated coupling based on a squaraine dye[J]. Advanced Materials, 2021, 33(26): 2100582.

[33] Gibert-Roca M, Molet P, Mihi A, et al. Near infrared organic photodetectors based on enhanced charge transfer state absorption by photonic architectures[J]. Journal of Materials Chemistry C, 2020, 8(28): 9688-9696.

P3HT∶Y6-Based Near-Infrared Organic Photomultiplication Photodetectors by Intermolecular Charge Transfer Effects

Hu Yifan[1], Hua Yulu[2], Ji Ting[1*], Shi Linlin[2], Cui Yanxia[2], Li Guohui[2**]

[1]*College of Physics, Taiyuan University of Technology, Taiyuan* 030024, *Shanxi, China*;

[2]*College of Electronic Information and Optical Engineering, Taiyuan University of Technology, Taiyuan* 030024, *Shanxi, China*

Abstract

Objective The photomultiplication organic photodetector based on trap-assisted carrier tunneling mechanism not only has high sensitivity but also simplifies system design and effectively improves the weak light detection performance of the photodetector. At present, photomultiplication organic photodetectors mainly focus on the visible range and have relatively few responses in the near-infrared region. Detection in the near-infrared region has broad application prospects in many fields and the demand is becoming increasingly urgent. Intermolecular charge transfer is a low-cost method for achieving near-infrared absorption in organic photomultiplier detectors, which can effectively expand the response band of devices. However, the absorption is low and the response is very weak at long wavelengths. The photomultiplication type devices can amplify weak photocurrent signals and improve device performance. Therefore, by introducing a small amount of organic acceptor Y6 in the P3HT active layer, we fabricate a photomultiplication type organic photodetector. Due to the intermolecular charge transfer between P3HT and Y6, the response band of the device can be extended to 1310 nm, which is superior to the reported near-infrared multiplication type organic photodetectors. By introducing an atomic level thickness of Al_2O_3 between the hole transport layer and the active layer, the device can work under both positive and negative biases. The external quantum efficiency of the device at 860 nm reaches 800%, with a detectivity of 5.6×10^{11} Jones. The external quantum efficiency of the device at 1310 nm reaches 80.4%, and the specific detectivity reaches 5.13×10^{10} Jones. This work can promote the development of near-infrared photomultiplication organic photodetector.

Methods Firstly, the cleaned ITO substrates are dried by nitrogen gas and transferred to a glove box. PEDOT∶PSS is diluted with anhydrous ethanol in a volume ratio of 1∶9 and is span-coated onto the ITO substrate to form a hole transport layer. Then, the Al_2O_3 interface modification layer is deposited by atomic layer deposition equipment. Subsequently, the active layer is formed by spin-coating P3HT∶Y6 mixture solution, with a P3HT and Y6 ratio of 100∶1 in weight. Finally, the Al electrode is deposited on the active layer by thermal evaporation. The bright and dark currents of the device are obtained by a digital source meter Keithley 2400 and different light sources in a sealed and room temperature state. The testing of external quantum efficiency and responsiveness is performed in a dark shielding box, with ITO as the anode connecting to the positive pole of the power supply and Al as the cathode connecting to the negative pole. The digital source meter Keithley 2400 is adopted to apply different voltages, and a femtosecond laser is utilized as the light source. The light intensity is attenuated to a specified size by an attenuation plate, and the dark current and bright state *J*-*V* curves under different light sources are collected. Finally, the external quantum efficiency and responsivity data are obtained through calculation (the data has been background deducted). The linear dynamic range, noise current, and specific detection rate of the device are tested, and the performance of the device is comprehensively analyzed. A spectrophotometer instrument is leveraged to characterize the ultraviolet visible near-infrared absorption spectrum. In addition, the transmission spectrum, reflection spectrum, and film thickness of the device are also tested.

Results and Discussions Al_2O_3 modified device with a structure of ITO/PEDOT∶PSS/Al_2O_3/P3HT∶Y6 (100∶1)/Al and a control device without Al_2O_3 are both fabricated. We verify that the Al_2O_3 interface modification layer can greatly reduce the dark current of the device and enable the device to achieve bidirectional bias response (Fig. 1). Next, the Al_2O_3 modified device is characterized, and the device can respond to 1310 nm. The weak light detection limit of the device at 505 nm can reach 7.8 nW/cm^2. When the optical power density is 3.8×10^{-4} mW/cm^2, the external quantum efficiency of the device at 860 nm is 800%, with a specific detectivity of 5.6×10^{11} Jones. When the optical power density is 3.67×10^{-2} mW/cm^2, the external quantum efficiency of the device at 1310 nm is 80.4%, with a specific detectivity of 5.13×10^{10} Jones. Under the irradiation of visible light at 505 nm and near-infrared light at 860 nm, the device has a dynamic range of over 125 dB and 90 dB, respectively (Fig. 2 and Fig. 3). The comprehensive performance of the device has certain advantages compared to the near-infrared organic photomultiplier detectors prepared in recent years. By introducing an organic receptor Y6 with light absorption ability in the near-infrared region, the device effectively promotes the injection of holes from external currents as an electron trap and interacts with P3HT, expanding the corresponding band and

achieving high sensitivity detection in the near-infrared region (Fig. 4).

Conclusions A low-cost and highly sensitive near-infrared photomultiplication organic photodetector with a structure of ITO/PEDOT∶PSS/Al_2O_3/P3HT∶Y6/Al is reported. By adding Al_2O_3 as an interface modification layer, the dark current of the device is significantly reduced, resulting in a device that can respond in both forward and reverse bias directions. Adding a small amount of Y6 to the active layer can achieve a wide spectral response from UV visible to near-infrared, and the response wavelength can be extended to 1310 nm. The external quantum efficiency of the device at 860 nm reaches 800%, with a specific detectivity of 5.6×10^{11} Jones. The external quantum efficiency of the device at 1310 nm reaches 80.4%, and the specific detectivity reaches 5.13×10^{10} Jones. These properties have certain advantages in reported near-infrared photomultiplication organic photodetector and can promote the development of near-infrared photomultiplication organic photodetectors.

Key words detectors; intermolecular charge transfer; near infrared waveband; photomultiplication organic photodetectors; bidirectional biases; interface modification